ELECTROMAGNETIC-MECHANICAL ANALYSIS OF THE RADIO FREQUENCY DIPOLE CRAB CAVITY FOR HIGH LUMINOSITY LARGE HADRON COLLIDER

O. Kononenko, Z. Li, C.-K. Ng
SLAC National Accelerator Laboratory, Menlo Park, USA
Oleksiy.Kononenko@slac.stanford.edu

Abstract

High Luminosity Large Hadron Collider (HL-LHC) is a project aiming to broaden the LHC discovery potential by increasing the luminosity by a factor of ten beyond the design value. Development of the superconducting rf crab cavities for maximizing and levelling the luminosity is one of the major activities under the proposed upgrade. Due to the narrow bandwidth, the operating voltage and phase are sensitive to Lorentz force and various external loads, so if not studied and controlled, the resulting detuning can lead to performance degradation of the crabbing scheme. The parallel ACE3P simulation suite has recently enabled realistic multiphysics characterization of such complex accelerator systems on supercomputers. Using ACE3P, we perform a 3D analysis of the electromechanical effects in the dressed rf dipole crab cavity, including the two-cavity chain, in order to assess the operational reliability of the cryomodule. The simulation results are compared with available measurements and their implications are discussed.

I. INTRODUCTION

The High Luminosity Large Hadron Collider (HL-LHC) project aims to broaden the LHC discovery potential after 2025 when the collider luminosity will be increased by a factor of ten beyond the design value [1]. For maximizing and leveling the luminosity, the superconducting rf (SRF) crab cavities will be used [2]. Radio frequency dipole (RFD) and double quarter wave (DQW) options, chosen for the upgrade [3], are now under development to demonstrate the feasibility of the crabbing scheme. They are designed to provide a transverse kick voltage of about 3.4 MV per cavity and will be installed in pairs, one cryomodule per beam, on each side of the LHC interaction point 1 and 5.

The voltage and phase stability requirement, to better than 100 V and 0.001° [4], respectively, is one of the major operational concerns that demands a precise control. If special attention is not paid, the detuning from the Lorentz force and external loads, including liquid helium pressure fluctuations, can lead to serious performance degradation of the scheme. The design of the control system and the mechanical tuner [5] can be aided by a comprehensive numerical analysis of the electromagnetic-mechanical interactions in the cryomodule including the coupling between the rf fields, the external loads and the deformations of the cavity shape. Studying the structural modes and their contribution to the net detuning is especially important, as the low frequency mechanical resonances should be avoided to minimize the cavity perturbation due to microphonics [4].

The massively parallel ACE3P simulation suite, that includes electromagnetic, thermal and mechanical modules for the integrated analysis of accelerator problems, has recently enabled the realistic multiphysics characterization of such complex accelerator systems at large scale on supercomputers [6, 7]. In this paper we use ACE3P to model the electromagnetic-mechanical effects for the dressed RFD crab cavity, including the two-cavity chain, in order to assess the operational reliability of the cryomodule. The presented numerical procedure is also equally applicable for the analysis of other SRF crab cavity designs.

The paper is organized as follows. Section II introduces the structural models of the RFD cryomodule, the dressed cavity and the two-cavity chain. Section III presents the rf model and the cavity response to the static Lorentz force and tuner loads. Section IV demonstrates the simulation

This material is based upon work supported by the U.S. Department of Energy,
Office of Science, under Contract No. DE-AC02-76SF00515.

results on the structural resonances as well as their coupling strength to the cavity detuning. Section V provides some insight into the rf frequency shift due to the helium pressure fluctuations. Finally, Section VI presents our conclusions.

II. STRUCTURAL AND SIMULATION MODELS OF THE DRESSED RFD CAVITY

In Fig. 1 the structural model of the cryomodule [9], that includes two RFD cavities equipped with the mechanical tuners, is shown. In Table 1 the list of the selected relevant parameters of the cavity is presented according to the specification [4, 8].

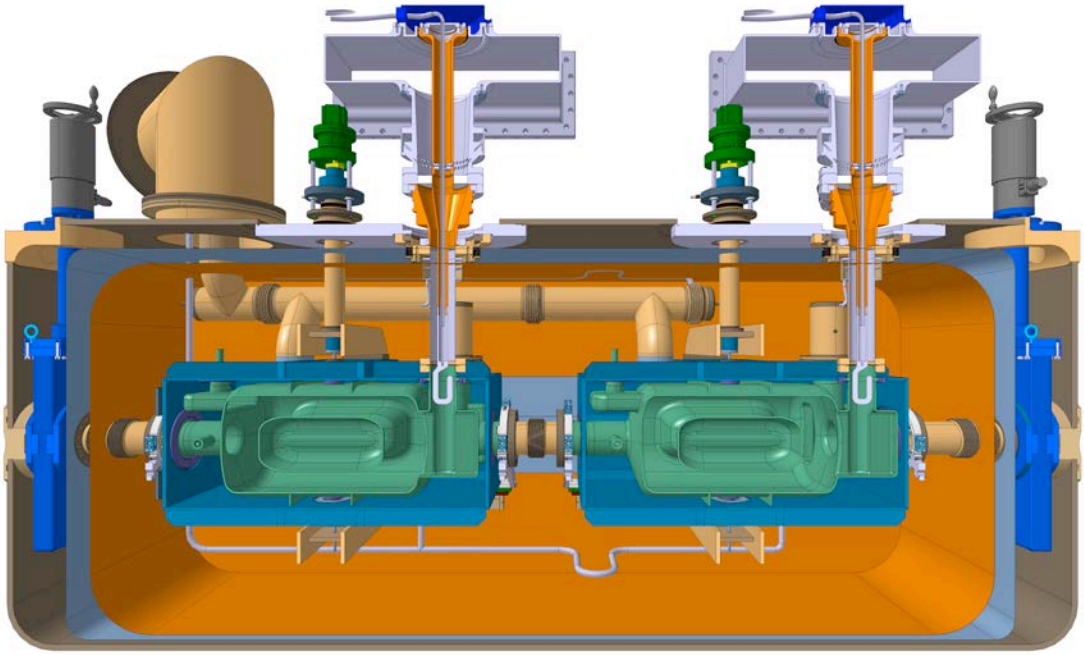

Figure 1. Longitudinal section of the cryomodule featuring two dressed RFD cavities equipped with the mechanical tuners.

Parameter	**Value**
RF frequency, f_0 [MHz]	400.79
Nominal kick voltage, V_x [MV]	3.4
Lorentz force detuning, k_{LF} [Hz/MV^2]	< 865
RF frequency sensitivity to He pressure, df/dp [Hz/mbar]	< 150
Operating temperature, T [K]	2

Table 1. Selected specification parameters relevant for the multiphysics analysis of the RFD cavity.

The cavity mechanical interaction with the external world is a function of a complex supporting geometry of the cryomodule and the tuning system not fully designed at the time of the study. The boundary conditions used for the dressed cavity simulations are therefore a simplification aimed at preserving the structural modes inside the helium tank and are chosen as follows: the beam-pipe flanges are fixed in transversal plane and free longitudinally, and the fundamental power coupler is fixed in all three directions.

The tuner tabs will be coupled through the frame attached to the bottom of the cavity and, at the top, to the motor through a tube. As the 3D model of the tuning system was not available at the

time of the study, we considered two options for the boundary conditions on the tabs: constrained vertically and, in particular for the comparison with the bare cavity tests [10], free in all the directions. The boundary conditions considered for the dressed cavity and the cavity materials [11] are illustrated in Fig. 2.

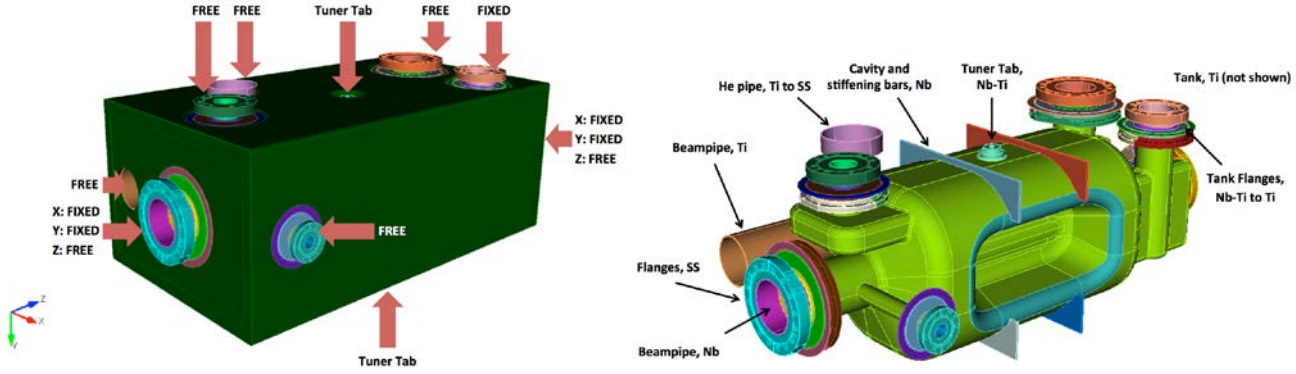

Figure 2. RFD crab cavity in a titanium tank showing the considered boundary conditions (left) and the dressed cavity materials (right).

The free connections, shown in Fig. 2 (left), were simplified and the helium tank was reconstructed based on the original drawings preserving the total mass and external dimensions. The resulting model of the RFD crab cavity is presented in Fig. 3 and the mechanical material properties are shown in Table 2 [12].

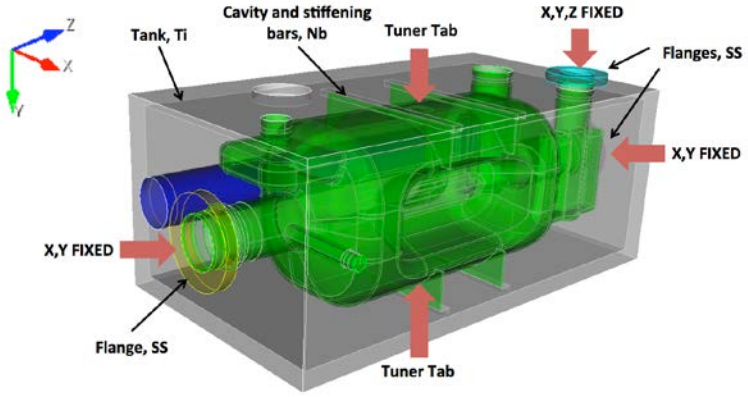

Figure 3. RFD crab cavity model used for the simulations featuring the boundary conditions and the materials involved.

Material	Density [kg/m^3]	Poisson Ratio	Young's Modulus [GPa]
Nb	8700	0.38	118
Nb-Ti	5700	0.33	68
Ti	4540	0.37	117
SS	8000	0.29	193

Table 2. Mechanical properties of the dressed cavity materials.

To assess the resonant modes of the coupled cavities within the cryomodule, we consider the two-cavity chain that is shown in Fig. 4. For this model we employ the same boundary conditions as

presented in Fig. 3, except for the flanges that are connected with the stainless steel inter-cavity bellows. The weak bellows for the second beam-pipe were not designed at the time of the simulation and were assumed to have a little impact on the resonant modes.

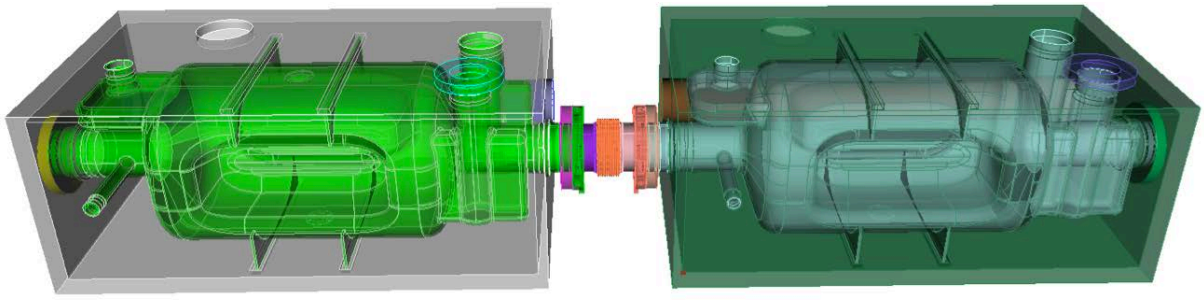

Figure 4. Two-cavity model showing a pair of the dressed cavities and the stainless steel inter-cavity bellows in between.

III. RF DETUNING FROM THE STATIC LORENTZ FORCE AND TUNER LOADS

To study the Lorentz force (LF) detuning, i.e. a frequency change due to the rf pressure on the cavity walls, first, we calculate the electromagnetic fields pattern for the 400 MHz operating mode in the cavity vacuum volume. $\vec{E}$ and $\vec{H}$, the amplitudes of the electric and magnetic fields, respectively, are shown in Fig. 5 as calculated with the Omega3P, the ACE3P rf eigenmode solver [13].

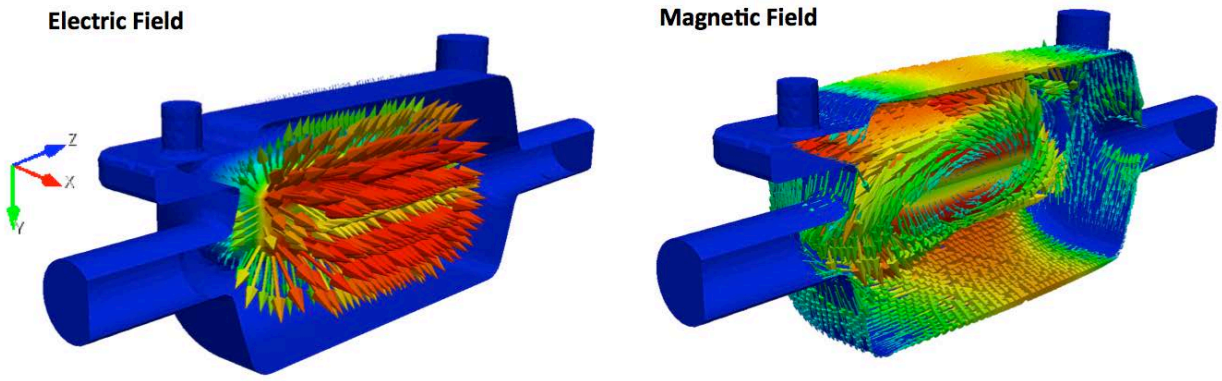

Figure 5. Direction and magnitude color-coded in a.u. on a linear scale for the electric (left) and magnetic (right) fields as calculated with ACE3P for the 400 MHz operating mode.

The RF pressure on the cavity walls, $\vec{t}_0$, was computed as $\vec{t}_0 = \frac{1}{4}\left(\mu_0\left|\vec{H}\right|^2 - \varepsilon_0\left|\vec{E}\right|^2\right)\vec{n}$, where ε_0 and μ_0 are the permittivity and permeability of the free space, respectively, and $\vec{n}$ is the normal to the cavity surface, see Fig. 6.

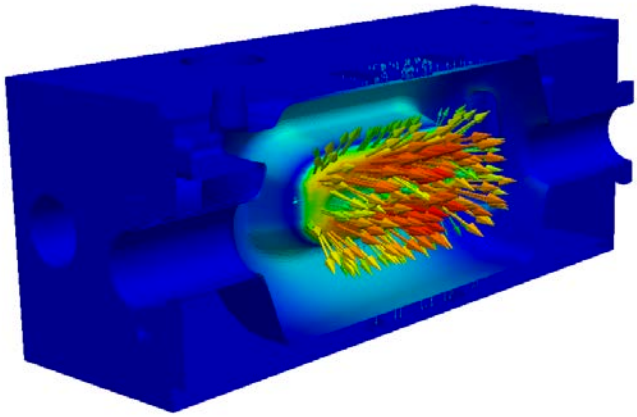

Figure 6. Direction and magnitude color-coded in a.u. on a linear scale for the electromagnetic pressure on the RFD cavity walls.

To normalize the calculated fields and the resulting electromagnetic pressure to V_x, the nominal kick voltage, two equivalent approaches both implemented in ACE3P could be used. First, by employing the Panofsky-Wenzel theorem [14] that couples the kick voltage V_x and the longitudinal voltage V_z for a given beam offset dx. Due to the field pattern, V_x is nearly constant as a function of dx in the vicinity of the beam, so the relation can be written as follows

$$V_z = -V_x \frac{\omega_0 dx}{ic}, \tag{1}$$

where c is a speed of light in vacuum and ω_0 is the angular frequency of the operating mode. For the V_z calculation only the electric field contributes, so the normalization becomes trivial. The second option is to calculate V_x directly from the fields on the beam axis, in this case the both electric and magnetic fields contribute, normalizing it to the 3.4 MV value.

Finally, the normalized rf pressure serves as a Neumann boundary condition on the cavity internal surface for the ACE3P multiphysics solver and the deformations due to the static Lorentz force are calculated for the following extreme cases: a) tuner tabs, shown in Fig. 3, are Y-fixed; b) tuner tabs are Y-free as in the bare cavity test [10]. The cavity displacements calculated for both cases are shown in Fig. 7 and 8, respectively.

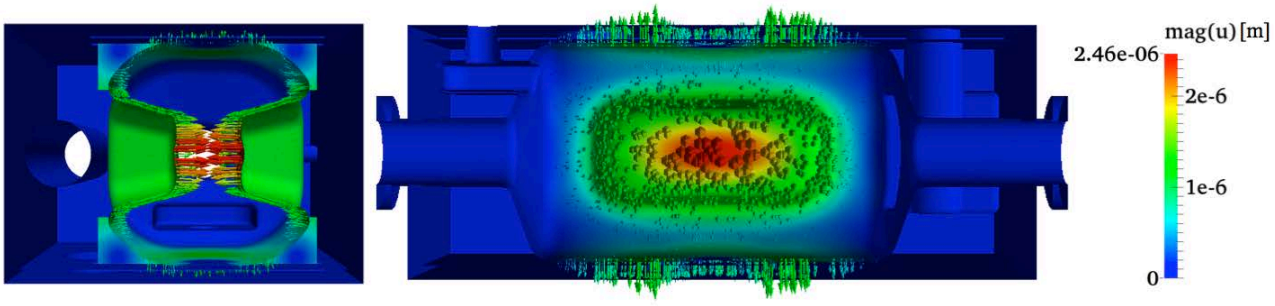

Figure 7. Direction and magnitude of the displacements of the dressed RFD cavity due to the static Lorentz force shown on transverse (left) and longitudinal sections (right), when the tuner tabs are constrained vertically, i.e. case a).

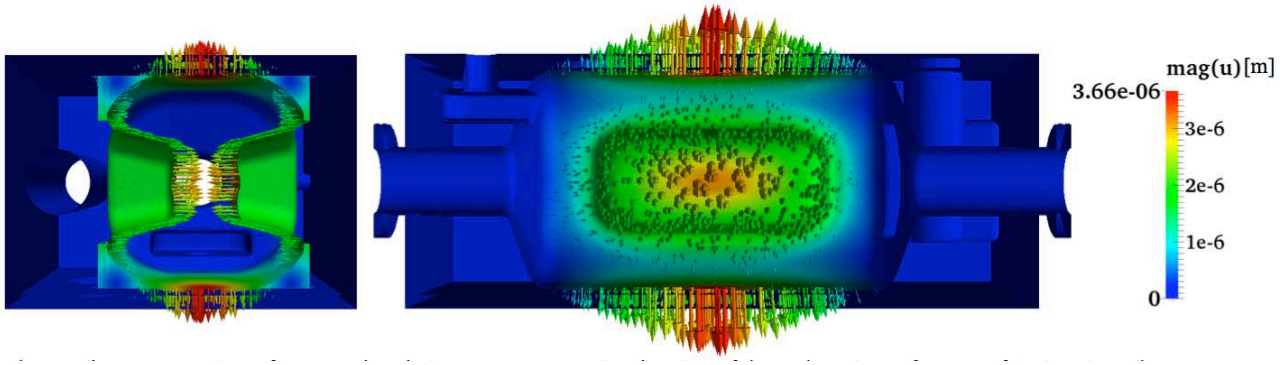

Figure 8. Direction and magnitude of the displacements of the dressed RFD cavity due to the static Lorentz force shown on transverse (left) and longitudinal sections (right), when the tuning tabs are free, i.e. case b).

The rf frequency shift due to the cavity deformations can now be computed by using the Slater's perturbation technique [15] as

$$\frac{\Delta f_0}{f_0} = \frac{\int_{\Delta V_{RF}} \left(\mu_0 \left|\vec{H}(x,y,z)\right|^2 - \varepsilon_0 \left|\vec{E}(x,y,z)\right|^2\right) dV_{RF}}{\int_{V_{RF}} \left(\mu_0 \left|\vec{H}(x,y,z)\right|^2 + \varepsilon_0 \left|\vec{E}x,y,z)\right|^2\right) dV_{RF}} \tag{2}$$

where Δf_0 is the frequency shift, V_{RF} is the unperturbed internal volume of the cavity, and ΔV_{RF} is the volume perturbation. Deforming the cavity vacuum model according to the structural deformations, the shifted frequency and the resulting Δf_0 can also be directly calculated from the Omega3P simulation on the perturbed mesh.

The frequency shift due to the Lorentz force, Δf_{LF}, and the coefficient normalized to the voltage $k_{LF} = \Delta f_{LF} / V_x^2$ as calculated for the above mentioned cases a) and b) are compared with the results from the ODU/JLab measurements for a bare cavity [10] in Table 3. For the case of the tuner tabs that are free, the calculated Δf_{LF} and the corresponding k_{LF} are in a good agreement with the data.

Boundary condition on the tabs	Δf_{LF} [Hz]	k_{LF} [Hz/MV^2]
a) Y-fixed	-6,639	-595
b) Y-free	-10,022	-898
ODU/JLab measurements	-8,623 to -9,780	-746 to -846

Table 3. RF detuning and the Lorentz force coefficients assuming different types of the boundary conditions on the tuner tabs as well as the ODU/Jlab data.

To compensate for the frequency shift, the tuning system is being designed for the crab cavities [5]. Simulating the cavity deformations due to the tuner load, the tuner tabs shown in Fig. 3 are "pushed" towards the cavity center imposing the symmetrical vertical displacement $dy = \pm 10$ μm on the top and the bottom cavity plates, respectively. The resulting structural displacements are shown in Fig. 9.

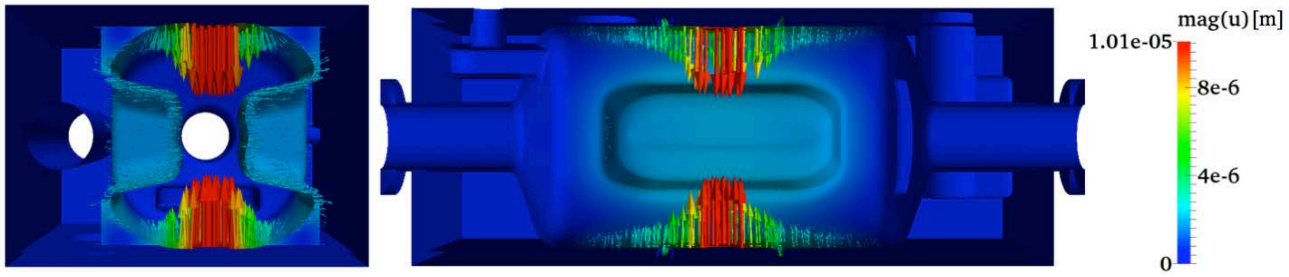

Figure 9. Direction and magnitude of the structural displacements of the dressed RFD cavity due to the static tuner load shown on the transverse (left) and the longitudinal sections (right).

The rf frequency change due to the tuner load, Δf_T, was calculated to be 10,594 Hz. The rf frequency sensitivity with the respect to the distance change between the top and bottom cavity plates was computed as $k_T = \Delta f_T / (2*|dy|) = 529$ Hz/μm. This is in some agreement with the tuning sensitivity reported in [5] and [16], that ranged from 345 to 1,000 Hz/μm. The spread in the results may be caused by the differences in the cavity models, including the shell thickness, changes of the mechanical material properties after the treatment or the assumptions for the boundary conditions.

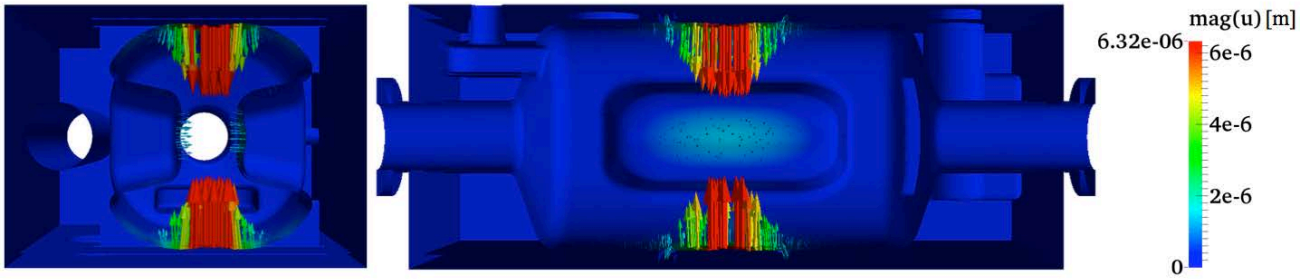

Figure 10. Direction and magnitude of the structural displacements of the dressed RFD cavity due to the tuner compensating for the Lorentz force, shown on transverse (left) and longitudinal sections (right).

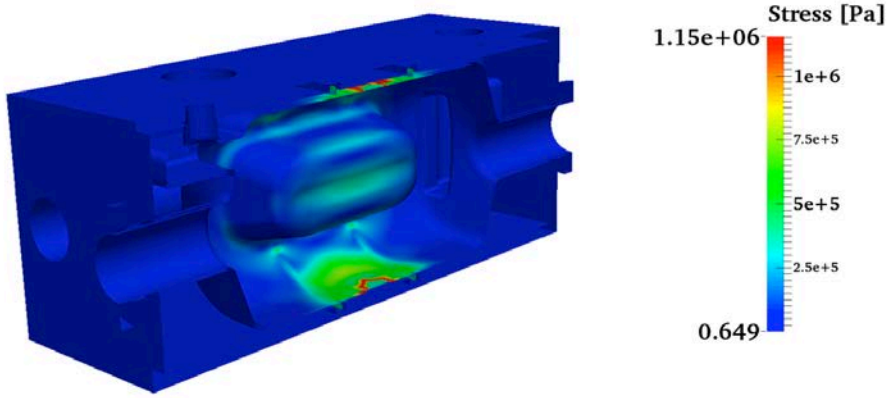

Figure 11. Von Mises stress on the cavity walls due to the tuner compensating for the Lorentz force.

As Δf_L and Δf_T have difference signs, the tuner displacement $dy = \Delta f_L / (2*k_T) \approx 6.3$ μm compensates for the frequency shift due to the static Lorenz force. This has been also confirmed through the coupled ACE3P rf-mechanical simulation. In Fig. 10 and Fig. 11 the displacements and Von Mises stress, respectively, are shown on the cavity walls, when the tuner compensates for the static Lorentz force tuning the cavity to the nominal rf frequency of 400 MHz. As expected, the maximum of the stress is localized around the tabs being well below the niobium yield strength [17].

IV. RESONANT MECHANICAL MODES OF THE DRESSED CAVITY

Using the ACE3P structural eigenvalue solver [18] we simulate the resonant modes of the dressed RFD cavity and the two-cavity chain, assuming two options for the boundary conditions as in the previous section: the tuner tabs are both fixed in Y or free. In Fig. 12 the frequencies of the lowest 20 modes are presented. As the mass of the liquid helium within the tank and other associated effects are not taken into account, these frequencies may be overestimated to some extent.

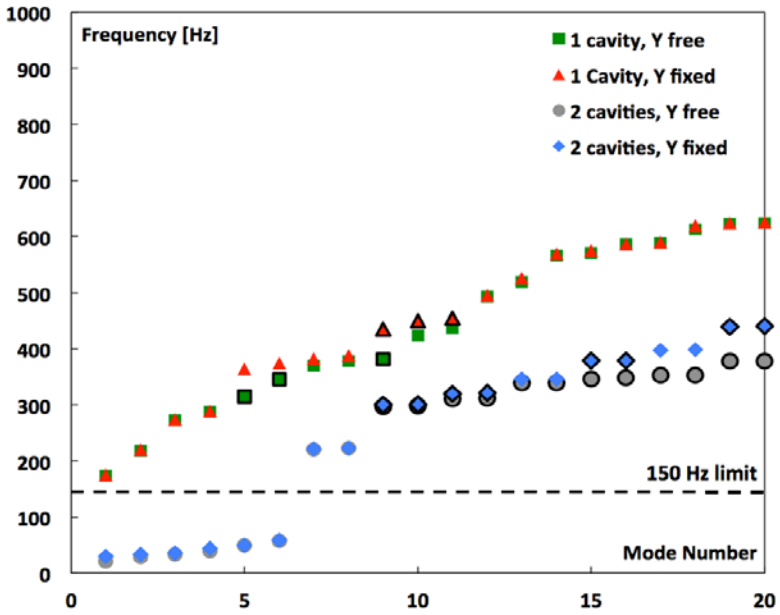

Figure 12. Frequencies of the lowest 20 modes for the RFD cavity in a tank (green and red) and the two-cavity chain (grey and blue). The cavity modes are highlighted.

According to [4], the mechanical resonances below 150 Hz should be avoided to minimize the cavity perturbations. As can be seen from Fig. 12, there are no cavity modes in this frequency range, however, once two cavities are coupled through the inter-cavity bellows, as is the case for the cryomodule, low frequency bellows and tank modes may appear.

Y free			Y fixed			
Mode Number	Frequency [Hz]	Δf_{LF} [Hz]	Mode Number	Frequency [Hz]	Δf_{LF} [Hz]	Δf_{T} [Hz]
3	273	-13	5	365	-4	9
4	288	-16	7	382	-3	6
6	**345**	**-7,990**	8	388	-9	17
7	370	-94	**9**	**435**	**-394**	**772**
8	378	-21	**10**	**450**	**-2,505**	**4,752**
9	381	-5	**11**	**454**	**-1,305**	**2,455**
10	424	-9	12	496	-17	29
Modal summation		-8,147	—	—	-4,235	8,039
Direct calculation		-10,022	—	—	-6,639	10,594

Table 4. The contribution of the modes to rf detuning identified by the spatial decomposition of the static Lorentz force and tuner displacements. Most dangerous resonances are bolded.

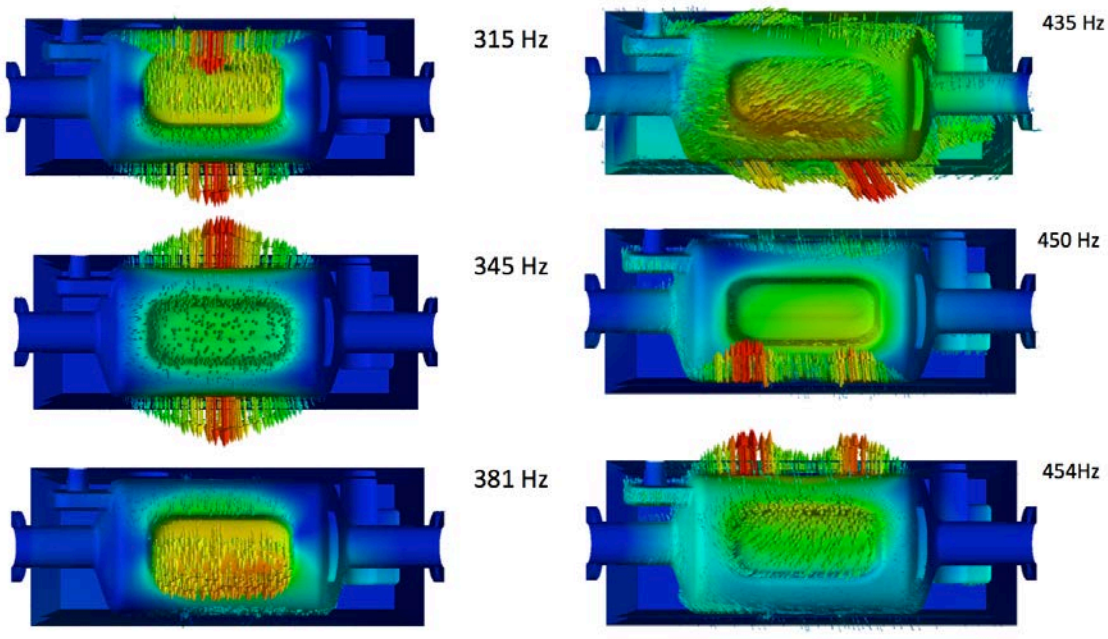

Figure 13. Direction and magnitude in a.u. on a linear scale of the displacements on the cavity walls for the selected mechanical modes, including the ones that may have the largest impact on the RF frequency, for two cases: tuner tab is Y free (left) and Y fixed (right).

If the gradient changes rapidly or external vibrations couple to the cavity, some of the mechanical modes may be excited. To study the mode strength, we perform the spatial decomposition of the static Lorentz force and tuner displacements [7], determining the contributions to the cavity detuning. In Table 4 the results of the decomposition are presented and the selected mode patterns are shown in Fig. 13. Some discrepancy between the static frequency shifts and the finite modal summations indicates that there are also some modes at higher frequencies that are unlikely to be excited during the operation.

As shown in Table 4, when the tuner tabs are free, the 345 Hz mechanical mode has the largest contribution to the detuning as symmetrically deforms the top and bottom cavity plates maximizing the volume perturbation in the sensitive region; the asymmetric vertical mode at 315 Hz, has a negligible contribution as the deformation of the top plate is compensated by the deformation of the bottom one; the horizontal modes, similar to 381 Hz one, also do not contribute a lot, see Fig. 13 (left). When the tuner tabs are constrained vertically, the modes at 435, 450 and 454 Hz significantly contribute to the detuning as they are associated with only one plate (top or bottom) of the cavity, see Fig. 13 (right).

All the contributing modes of the dressed RFD cavity are well above 150 Hz, and are unlikely to be excited by the external mechanical vibrations. However, if the gradient changes rapidly, or there is a pressure jump in the liquid helium coupling at the resonant frequencies, the modes may have a significant impact on the cavity performance.

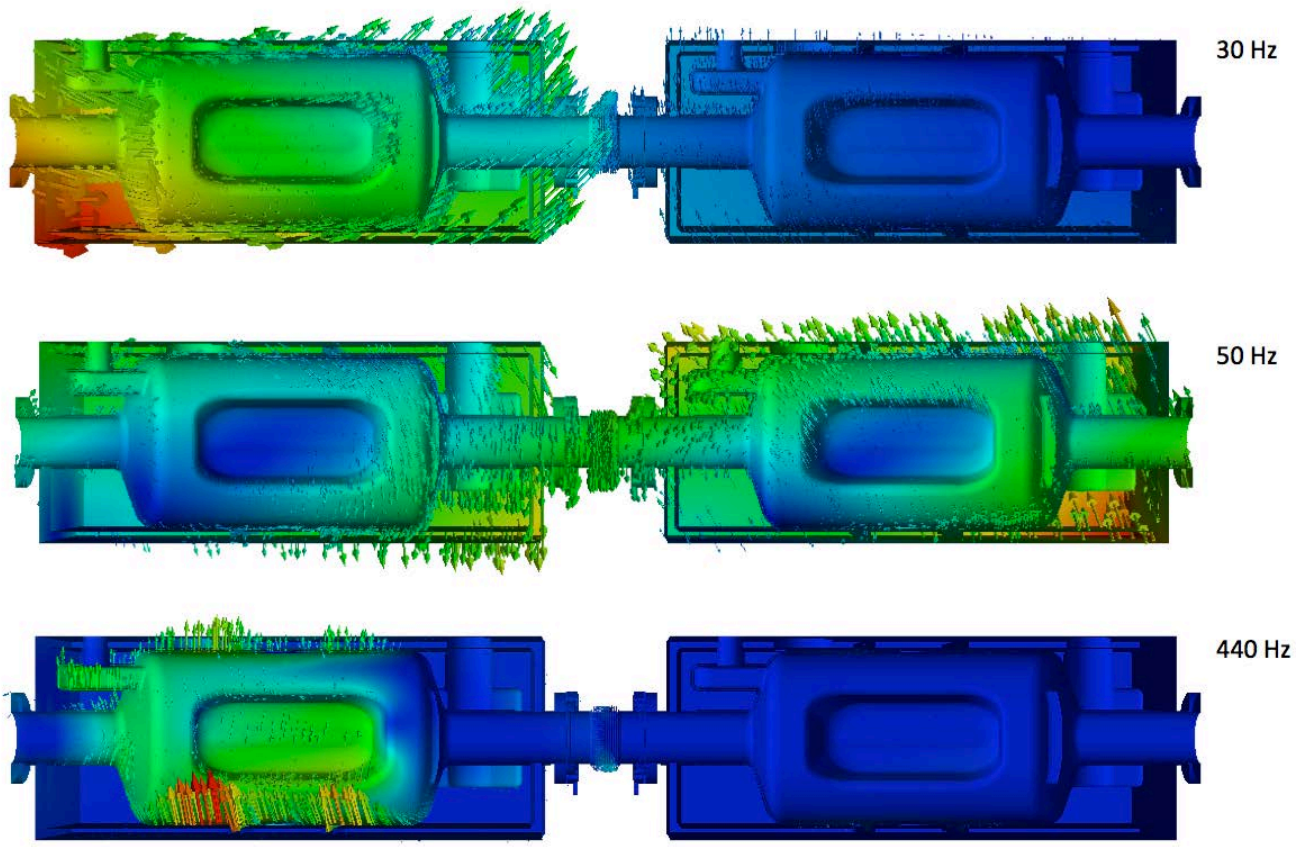

Figure 14. Direction and magnitude in a.u. on a linear scale of the displacements for the selected two-cavity chain mechanical modes when the tuner tab is Y-fixed.

On the other hand, for the two-cavity chain there are several modes with the frequencies below 150 Hz. Even though these are not the cavity modes, they may still have some effect on the detuning, see Fig. 14 (top and middle). The resonant modes having significant contribution to the cavity frequency shift are also present in the two-cavity chain spectrum at the similar frequencies. For instance, the mode at 440 Hz, see Fig. 14 (bottom), corresponds to the one at 450 Hz shown in Fig. 13 (right-middle).

V. DETUNING DUE TO THE CHANGES IN THE LIQUID HELIUM PRESSURE

The changes in the liquid helium pressure can detune the cavity significantly if uncontrolled. To calculate the df, frequency shift due to the pressure change of dp, we impose a load on the external cavity surface and compute the rf detuning. In Fig. 15 the structural displacements resulting from the external pressure of 1 mbar are shown.

In Table 5, the pressure sensitivity coefficient, df/dp, is presented as calculated for the Y-fixed and Y-free cases for the boundary conditions on the tuner tabs, as well as computed for the tuner stiffness of 6.8 kN/mm [19] and as measured for a bare cavity [20]. It is noted that the Y-free and Y-fixed values bound the case when the finite tuner stiffness was taken into account. Also, the df/dp appeared to be very sensitive to the boundary conditions on the tabs that change volume deformation in the high magnetic field regions, see Eq. (2). This suggests that the bare cavity measurements may not be directly applicable to the cavity equipped with the tuner.

Boundary condition on the tabs	df/dp [Hz/mbar]
a) Y-fixed	-288
b) Y-free	-130
c) 6.8 kN/mm tuner stiffness [19]	-147
ODU/JLab measurements	-42 to -59

Table 5. RF frequency sensitivity to the pressure change assuming different types of the boundary conditions on the tuner tabs as well as the ODU/Jlab data for a bare cavity.

The |df/dp| that was measured for two bare cavity prototypes at ODU/JLab is significantly smaller from the value calculated for the Y-free case. This can be explained by some differences in the boundary conditions for the cavity installed in the vertical test stand during the measurements and in the cryomodule, as is the case considered in this paper. It also means that a special attention is required for the pressure sensitivity coefficient not to exceed the specification limit of 150 Hz/mbar (see Table 1).

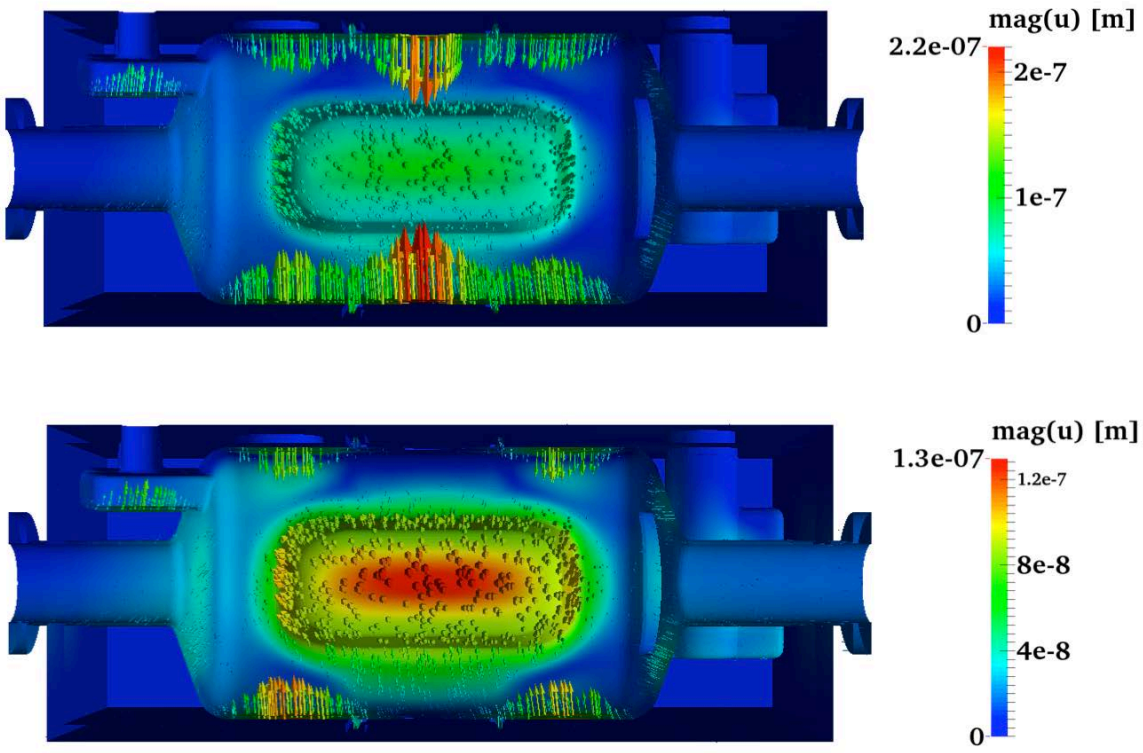

Figure 15. Direction and magnitudes of the structural displacements due to 1 mbar external pressure for two cases: tuner tabs are free (top) and fixed vertically (bottom).

VI. CONCLUSION

Comprehensive electromagnetic-mechanical analysis has been performed for the dressed RFD crab cavity in a helium vessel and the two-cavity chain, including the Lorentz force detuning effects, rf frequency sensitivity to the loads from the tuner and helium pressure, as well as the mechanical resonances and their contribution to the rf frequency change. The results are in fair agreement with

available experimental and simulation data, although the model considered may clearly have some limitations.

It was found that the mechanical modes that have the largest impact on the cavity detuning are the modes of the top and bottom cavity plates being well above the 150 Hz limit set in [4]. However, for the two-cavity chain some modes with a very small coupling to the cavities have also been identified. Also, the df/dp calculated was quite sensitive to the boundary conditions on the tuner tabs, meaning that the bare cavity measurements may not be directly applicable to the cavities equipped with the tuner and installed in a cryomodule.

As the complicated cavity supports, tuning mechanism and other elements were not fully designed at the time of the simulation, the results presented in the paper are preliminary, though still providing the useful input for the cryomodule and control system development.

VII. ACKNOWLEDGEMENT

We would like to thank to our colleagues within the HL-LHC collaboration for their invaluable help. This research used resources of the National Energy Research Scientific Computing Center, which is supported by the Office of Science of the U.S. Department of Energy under Contract No. DE-AC02-05CH11231.

VIII. REFERENCES

[1] The High Luminosity LHC Project, http://hilumilhc.web.cern.ch
[2] R. Calaga, Crab cavities for the LHC upgrade, in Proc. Workshop on LHC, Chamonix, France, 2012, pp. 363-372.
[3] High-Luminosity Large Hadron Collider (HL-LHC). Preliminary Design Report, edited by G. Apollinari, I. Béjar Alonso, O. Brüning, M. Lamont, L. Rossi, CERN–2015–005 (CERN, Geneva, 2015), DOI: http://dx.doi.org/10.5170/CERN-2015-005
[4] High-Luminosity Large Hadron Collider (HL-LHC). Technical Design Report V. 0.1, edited by G. Apollinari, I. Béjar Alonso, O. Brüning, P. Fessia, M. Lamont, L. Rossi, L. Tavian, CERN Yellow Reports: Monographs, Vol. 4/2017, CERN-2017-007-M (CERN, Geneva, 2017). https://doi.org/10.23731/CYRM-2017-004
[5] K. Artoos et al., Development of SRF cavity tuners for CERN, in Proc. 17th Int. Conf. on RF (SRF'15), Whistler, BC, Canada, 2015, pp. 1247-1251.
[6] ACE3P simulation suite, https://portal.slac.stanford.edu/sites/ard_public/acd/Pages
[7] O. Kononenko, C. Adolphsen, Z. Li, C.-K. Ng, and C. Rivetta, 3D multiphysics modeling of superconducting cavities with a massively parallel simulation suite, Physical Review Accelerators and Beams, Vol. 20, 102001, 2017.
[8] Dressed RFD cavities functional requirements specification, Prepared by L. Ristori, LHC-ACFDC-ES-0001, 2017.
[9] C. Zanoni et al., EN-MME Crab Cavity Meeting, 2014, https://indico.cern.ch/event/351679/
[10] S. De Silva, RFD Experience for SPS and Evolution to LHC, International Review of the Crab Cavity Performance for HiLumi, April 3-5, 2017.
[11] C. Zanoni and HyeKyoung Park, private communications.
[12] Material properties for engineering analyses of SRF cavities, Fermilab Specification: ED0371110, 2013, 54 pages.
[13] L.-Q. Lee, Z. Li, C. Ng, K. Ko, Omega3P: A Parallel Finite-Element Eigenmode Analysis Code for Accelerator Cavities, SLAC-PUB-1352, 2009, 7 pages.
[14] W. K. H. Panofsky and W. A. Wenzel, Some considerations concerning the transverse deflection of charged particles in radio-frequency fields, Rev. Sci. Instrum., vol. 27, p. 967, 1956.

[15] J. C. Slater, “Microwave Electronics,” Rev. Mod. Phys., Vol. 18, No. 4, 441(1946).
[16] HyeKyoung Park, RFD Cavity Frequency Fix Plan, SRF Engineering Meeting, JLAB, 2016, https://indico.cern.ch/event/546116/sessions/201715/attachments/1298352/1936893/ODU-JLAB-RFD-Frequency_fix_plan-Jun16.pdf
[17] C. Antoine, M. Foley, N. Dhanaraj, Physical properties of niobium and specifications for fabrication of superconducting cavities, TD-06-048, FNAL, 2006.
[18] O. Kononenko et al., A Massively Parallel Finite-Element Eigenvalue Solver for Modal Analysis in Structural Mechanics, SLAC-PUB-16229, 2014, 15 pages.
[19] P. Berutti, RFD design update, US-UK-CERN Crab cavity coordination meeting, Geneva, Switzerland, Novermber 2017, https://indico.cern.ch/event/679916/
[20] J. Delayen, Experimental Results for US RFD Cavities, the HL-LHC Collaboration Meeting Madrid, Spain, 2017,
https://indico.cern.ch/event/647714/contributions/2651548/attachments/1557276/2449591/HL-LHC_Meeting_Madrid_2017-RF_Dipole-JRD.pdf